

On the two high-metallicity DLAs at $z = 2.412$ and $z = 2.583$ towards Q 0918+1636 ^{*}

J. P. U. Fynbo^{1,†}, S. J. Geier^{1,2}, L. Christensen¹, A. Gallazzi^{3,1}, J.-K. Krogager^{1,4},
T. Krühler¹, C. Ledoux⁴, J. R. Maund^{5,6}, P. Møller⁷, P. Noterdaeme⁸,
T. Rivera-Thorsen^{1,9}, M. Vestergaard^{1,10}

¹Dark Cosmology Centre, Niels Bohr Institute, Copenhagen University, Juliane Maries Vej 30, 2100 Copenhagen O, Denmark

²Nordic Optical Telescope, Apartado 474, 38700 Santa Cruz de La Palma, Spain

³INAF – Osservatorio Astrofisico di Arcetri, Largo Enrico Fermi 5, 50125 Firenze, Italy,

⁴European Southern Observatory, Alonso de Córdova 3107, Vitacura, Casilla 19001, Santiago 19, Chile

⁵Astrophysics Research Centre, School of Mathematics and Physics, Queen's University Belfast, Belfast BT7 1NN, UK

⁶Royal Society Research Fellow,

⁷European Southern Observatory, Karl-Schwarzschildstrasse 2, 85748 Garching bei München, Germany

⁸Institut d'Astrophysique de Paris, CNRS-UPMC, UMR7095, 98bis bd Arago, 75014 Paris, France

⁹Department of Astronomy, AlbaNova, Stockholm University, 106 91 Stockholm, Sweden

¹⁰Steward Observatory, University of Arizona, 933 North Cherry Avenue, Tucson, AZ 85721

17 September 2018

ABSTRACT

The quasar Q0918+1636 ($z = 3.07$) has two intervening high-metallicity Damped Lyman- α Absorbers (DLAs) along the line of sight, at redshifts of $z = 2.412$ and 2.583 . The $z = 2.583$ DLA is located at a large impact parameter of 16.2 kpc, and despite this large impact parameter it has a very high metallicity (consistent with solar), a substantial fraction of H_2 molecules, and it is dusty as inferred from the reddened spectrum of the background QSO. The $z = 2.412$ DLA has a metallicity of $[M/H] = -0.6$ (based on ZnII and SiII). In this paper we present new observations of this interesting sightline consisting of deep multi-band imaging and further VLT spectroscopy. By fitting stellar population synthesis models to the photometric SED we constrain the physical properties of the $z = 2.583$ DLA galaxy, and we infer its morphology by fitting a Sersic model to its surface brightness profile. We find it to be a relatively massive ($M_* \approx 10^{10} M_\odot$), strongly star-forming ($SFR \approx 30 M_\odot \text{ yr}^{-1}$), dusty ($E_{B-V} = 0.4$) galaxy with a disk-like morphology. We detect strong emission lines from the $z = 2.583$ DLA ([OII] $\lambda 3727$, [OIII] $\lambda 4960$, [OIII] $\lambda 5007$, H β , and H α , albeit at low signal-to-noise (S/N) ratio except for the [OIII] $\lambda 5007$ line). The metallicity derived from the emission lines is consistent with the absorption metallicity ($12 + \log(O/H) = 8.8 \pm 0.2$). We also detect [OIII] $\lambda 5007$ emission from the galaxy counterpart of the $z = 2.412$ DLA at a small impact parameter (< 2 kpc). Overall our findings are consistent with the emerging picture that high-metallicity DLAs are associated with relatively luminous and massive galaxy counterparts, compared to typical DLAs.

Key words: galaxies: formation – galaxies: high-redshift – galaxies: ISM – quasars: absorption lines – quasars: individual: SDSS J091826.16+163609.0 – cosmology: observations

* Based on observations carried out under prog. ID 084.A-0303 and 089.A-0087 with the X-Shooter spectrograph installed at the Cassegrain focus of the Very Large Telescope (VLT), Unit 2 – Kueyen, operated by the European Southern Observatory (ESO) on Cerro Paranal, Chile. Based on observations made with the NASA/ESA Hubble Space Telescope, obtained at the Space Telescope Science Institute, which is operated by the Association of Universities for Research in Astronomy, Inc., under NASA contract NAS 5-26555. These observations are associated with program 12553.

Based on observations made with the Nordic Optical Telescope, operated on the island of La Palma jointly by Denmark, Finland, Iceland, Norway, and Sweden, in the Spanish Observatorio del Roque de los Muchachos of the Instituto de Astrofísica de Canarias.

† E-mail: jfynbo@dark-cosmology.dk

1 INTRODUCTION

For a long time the only available method for studying galaxies at redshifts $z > 1$ (barring QSO host galaxies) was to look at them in absorption against the light of background QSOs (e.g., Weymann et al. 1981; Wolfe et al. 2005). Then, from the second half of the 1990ies, the study of high- z galaxies in emission went through a breakthrough that is still unfolding (e.g., Giavalisco 2002; Shapley 2011). However, combining the information from absorption and emission lines is still a poorly developed field. Although more than 10 000 of the so-called Damped Lyman- α Absorbers (DLAs) have been found so far (Noterdaeme et al. 2012b), and despite some progress (e.g., Møller et al. 2002) in finding their galaxy counterparts, we still have less than a dozen examples of such absorption selected galaxies (Krogager et al. 2012, see also Rauch et al. 2008, Rauch & Haehnelt 2011 and Schulze et al. 2012).

Expanding the sample is of great interest as we in this manner obtain unique information about the kinematics and chemical composition of gas surrounding the central ~ 1 kpc which are typically studied in emission. This information is vital for probing current ideas about the role of processes like inflow of pristine gas and outflow of enriched gas in galaxy formation and evolution (e.g., Dekel et al. 2009; Bouché et al. 2010; Fumagalli et al. 2011; Dekel & Krumholz 2013; Crighton et al. 2013, and references therein).

The $z = 3.07$ quasar SDSSJ091826.16+163609.0 was selected in the survey for high-metallicity DLAs described in Fynbo et al. (2010) and Fynbo et al. (2011). It was selected due to the presence of a DLA at $z = 2.412$ with strong FeII lines. After obtaining deep X-Shooter spectroscopy of the QSO, Fynbo et al. (2011) serendipitously discovered a second DLA at $z = 2.583$ along the line of sight with even stronger metal lines. Fynbo et al. (2011) detected the forbidden [OII] and [OIII] emission lines of the galaxy counterpart of this second DLA. The galaxy is located at an impact parameter of $2''$, corresponding to ~ 16 kpc at $z = 2.583$. The $z = 2.412$ DLA was not detected in emission in that study.

In this paper, we present new results based on new observations of this sightline obtained with the Hubble Space Telescope (*HST*), ESO Very Large Telescope (VLT) and Nordic Optical Telescope (NOT). In Sect. 2 we give an overview of the observations and data reduction, and describe the data analysis and the results in Sect. 3 and Sect. 4. Finally, Sect. 5 contains a discussion of our findings and their implications for the field.

Throughout this paper, we use a flat Λ CDM cosmology with $\Omega_\Lambda = 0.728$, $\Omega_m = 0.272$ and a Hubble constant of $H_0 = 70.4 \text{ km s}^{-1} \text{ Mpc}^{-1}$ (Komatsu et al. 2011). All magnitudes are given in the AB system.

2 OBSERVATIONS AND DATA REDUCTION

2.1 HST imaging

The field of Q0918+1636 was observed with the Wide Field Camera 3 (WFC3) on the *HST* on two epochs in November 2011 (with the NIR detector in the F105W and F160W filters) and on April 18 2012 (with the UVIS detector in the F606W filter). The roll-angle of the telescope was set such that the $z = 2.583$ DLA galaxy falls between the diffraction spikes of the Point Spread Function (PSF) of the QSO. The two observations with the NIR detector were taken using the WFC3-IR-DITHER-BOX-MIN pattern providing an optimal 4-point sampling of the PSF. The UVIS observation was taken using the WFC3-UVIS-DITHER-BOX pattern.

Table 1. Log of observations

Band	Obs. Date	Exp. Time (sec)
<i>HST</i> /WFC3/F105W	Nov 9 2011	2612
<i>HST</i> /WFC3/F160W	Nov 9 2011	2612
<i>HST</i> /WFC3/F606W	Apr 9 2011	2523
NOT/Alfosc/g	Jan 25–26 2012	8400
NOT/Alfosc/u	Jan 25–26 2012	11500
NOT/NOTCam/ K_s	Mar 3 2012	7830
VLT/X-Shooter ¹ stare PA=0°	Feb 16 2010	3600
VLT/X-Shooter ¹ stare PA=60°	Feb 16 2010	3600
VLT/X-Shooter ¹ stare PA=-60°	Feb 16 2010	3600
VLT/X-Shooter nod PA=-66°	Apr 15 2012	2920
VLT/X-Shooter stare PA=162°	Apr 15 2012	6400
VLT/X-Shooter nod PA=66°	Mar 15–16 2013	10800

(¹) Already published in Fynbo et al. (2011).

We have reduced and combined the images using the software package `multidrizzle` provided by the STScI. By shifting and combining the images taken with sub-pixel offsets one achieves a better sampling of the PSF, which in the case of the IR observations is crucial as the PSF is poorly sampled in the native $0''.13 \text{ px}^{-1}$ images. For this work we have set the parameter `pixfrac` to 0.7 in all reductions and used a final pixel scale of $0''.06 \text{ px}^{-1}$ for IR and $0''.024 \text{ px}^{-1}$ for UVIS. For a detailed description of the parameters in the software we refer to the `multidrizzle` user manual.

2.2 NOT imaging

On the nights of Jan 25–26 2012 and March 3 2012 Q0918+1636 was observed with the Andalucia Faint Object Spectrograph and Camera (ALFOSC) and with the Nordic Optical Telescope near-infrared Camera and spectrograph (NOTCam) at the NOT. A total of 8400 s, 11500 s and 7830 s of exposure time was obtained in the g -band, u -band, and K_s -band, respectively (see Table 1). Observing conditions were clear, with an average seeing FWHM of $\sim 1''$ in the January 2012 nights, and clear and sub-arcsec seeing on March 3rd 2012. The optical images were reduced using IRAF¹ standard procedures. The NOTCam images were reduced with custom IDL scripts, using a running-median for sky-subtraction, and an object mask for 2nd pass sky-subtraction. The NOTCam distortion correction was applied using the IRAF/`geotran` task.

2.3 VLT/X-Shooter spectroscopy

Q0918+1636 was observed with VLT/X-Shooter on April 15 2012. Both a stare observation at a position angle of 162° East of North and a nodding observation at a position angle of -66° East of North were obtained. The observation at position angle -66° East of North was a mistake: it should have been at 66° East of North with the purpose of covering the $z = 2.583$ DLA galaxy and the QSO. In a stare observation the target is kept at a fixed position on

¹ IRAF is distributed by the National Optical Astronomy Observatory, which is operated by the Association of Universities for Research in Astronomy (AURA) under cooperative agreement with the National Science Foundation.

the slit throughout the observation, whereas in a nodding observation an observing block consists of four exposures between which the target is moved in an ABBA pattern along the slit. A deeper observation was obtained on March 15–16 2013 at the correct position angle of 66° East of North for covering the $z = 2.583$ DLA galaxy and the QSO using the nodding template with a nod-throw of $4''$. In Fig. 1 we show the orientation of the slits in all the X-Shooter observations, both the new observations reported here and the previous observations of Fynbo et al. (2011). The purpose of the stare observation at position angle of 162° East of North was to determine the redshift of the galaxy seen in the bottom of Fig. 1 in order to establish if this could be the galaxy counterpart of the $z = 2.412$ DLA. For the full log of observations we refer to Table 1.

The spectra from March 2013 were reduced with the ESO X-Shooter pipeline 2.0 (Modigliani et al. 2010; Goldoni 2011). We use the default parameters for the first five recipes which perform the basic calibrations (master darks, order prediction, flat fields, and the 2D maps for later rectification of the spectra). For the reduction of the object frames we use the corresponding pipeline recipes for the stare and nodding modes, with parameters optimized to provide the best possible sky-subtraction. The flux standard star LTT3218 was observed in both nights. Those spectra were reduced with the same calibration data as the spectra of the QSO/DLA system, and sampled onto the same spatial and wavelength grid. The extracted 1-dimensional (1D) standard star spectra were divided by the known tabulated spectrum of the standard star (which is first interpolated to the same wavelength grid), and the result smoothed with a kernel of 30 pixels to obtain a clean response curve. Each individual 2D spectrum was first normalized to an integration time of 1s, and then divided by the also normalized response curve from the corresponding night. The resulting flux-calibrated spectra from the 3 individual observing blocks (each comprising one hour of integration time) were collapsed along the wavelength axis to determine the peak positions of their spectral PSFs (SPSFs), and subsequently aligned on the spatial axis. Thereafter, they were stacked by means of a median combination. Galactic extinction corrections were taken from Schlafly & Finkbeiner (2011)² and implemented with the *fm_unred* code in IDL. The final SPSF was determined by collapsing the error-weighted 2D stack along the wavelength axis in the *H*-band wavelength range and the 1D spectrum of the quasar itself was extracted by applying the corresponding normalized weights, similar to the optimal extraction procedure described in Horne (1986). To check the flux level we integrated the 1D spectrum over the transmission curves of the NOTCam *J*- and *H*-band filters, and compared with the photometry from Fynbo et al. (2013). The measurements agree within the errorbars, thus no correction of the flux level was necessary. With a gaussian fit to the SPSF we determined the seeing of the combined spectrum to be $\sim 0''.8$ in the *H*-band.

3 THE $z = 2.583$ DLA GALAXY

3.1 HST imaging

Based on the high resolution HST imaging we can now improve the relative astrometry over that presented in Fynbo et al. (2011). We find that the DLA galaxy is located at an impact parameter of 1.98 ± 0.02 arcsec from the QSO at a position angle of -115° East

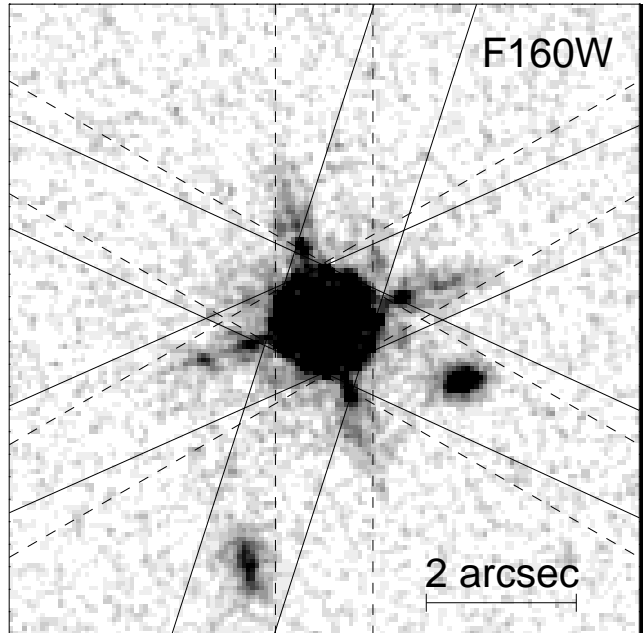


Figure 1. The *HST*/WFC3 F160W image and with all the X-Shooter slit orientations indicated with dashed lines for the observations presented in Fynbo et al. (2011) and full-drawn lines for the new observations presented here (see also Table 1).

of North, consistent with the earlier measurements. This impact parameter corresponds to a proper distance of 16.2 kpc at $z = 2.583$.

We used the GALFIT tool (Peng et al. 2002; Peng 2010) to fit 2D Sersic models, convolved with the PSF, to the HST images of the DLA galaxy. The Point Spread Functions (PSFs) for the *HST* images were simulated using the software TINYTIM. We chose to simulate the PSFs instead of using an empirical PSF as the model PSF has higher S/N ratio in the outer parts, where the PSFs from the data have high noise due to the background. We did the PSF simulation by first creating models using TINYTIM for each position of the target in the four-point dither pattern, assuming a QSO spectrum for the wavelength dependent PSF modelling, and taking into account the aberrations of the telescope as specified in the auxiliary data files. The models were sub-sampled by a factor of 5 compared to the native pixel scale of the detectors in order to position the model PSF more accurately. We then re-sampled the model PSF images to the native sampling and convolved them with the appropriate filter-specific Charge Diffusion Kernel. The four “raw” PSF images were then combined by the pipeline task *multidrizzle* in IRAF using the same parameters as for the data reduction. This allows us to mimic the effects of the reduction procedures. The results from GALFIT are the best-fit values for the effective half-light radius r_{eff} , the Sersic index n , and the axis ratio $\frac{b}{a}$, which quantify the structure of the galaxy. The circularized radius is calculated as $r_c = r_{\text{eff}} \cdot \sqrt{\frac{b}{a}}$.

GALFIT also delivered photometry in all three bands, summarized in Table 2. Galactic extinction corrections are taken from the Schlafly & Finkbeiner (2011) maps.

The $z = 2.583$ DLA galaxy has a disk-like morphology with a Sersic index consistent with 1. The galaxy is compact with a circularized radius of only $0.11''$ corresponding to 0.9 kpc.

² provided by <http://ned.ipac.caltech.edu/>

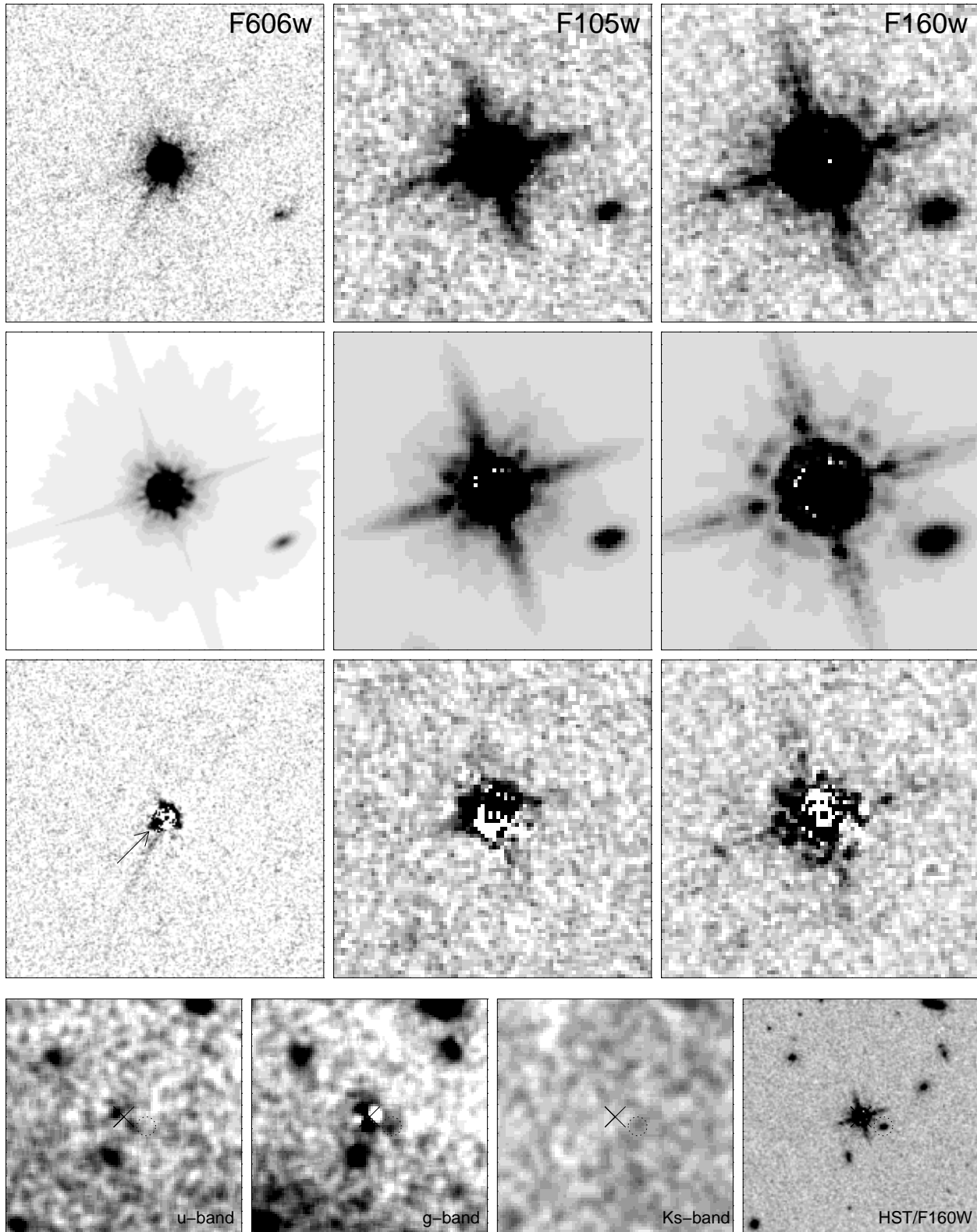


Figure 2. Top 9 panels: 5×5 arcsec² sections centred on the QSO in F606W, F105W and F160W (from left to right). The DLA galaxy is seen south-west of the QSO at an impact parameter of $2''$. The top row shows the science images, the middle row shows the GALFIT model and the bottom row shows the residuals after subtracting the model (QSO PSF and galaxy models) from the science images. The field size is 5×5 arcsec² and the images are oriented with North up and East to the left. The arrow in the lower left panel indicates the possible signature of the $z = 2.412$ DLA galaxy. The tail extending below the QSO is a result of Charge Transfer Inefficiency. Bottom panel: 19×19 arcsec² sections centred on the QSO in the u-, g-, and Ks-bands after PSF-subtraction. Also shown to the right is the *HST*/F160W band image on the same scale for comparison. The position of the $z = 2.583$ DLA galaxy is marked with a dotted circle. Again the images are oriented with North up and East to the left.

Table 2. Results from the GALFIT fits and NOT photometry. b/a is the ratio of the minor and major axis radii and n is the Sersic index. The magnitudes in the HST filters were computed by GALFIT, whereas aperture photometry was done on the NOT images.

Band	mag (AB)	r_{eff} (kpc)	PA (deg)	b/a	n	r_c (kpc)
F606W	25.46 ± 0.13	1.2 ± 0.2	-37 ± 6	0.4 ± 0.1	0.8 ± 0.4	0.73
F105W	24.61 ± 0.09	1.3 ± 0.3	-44 ± 9	0.3 ± 0.2	0.1 ± 0.7	0.69
F160W	23.68 ± 0.06	1.4 ± 0.1	-47 ± 6	0.4 ± 0.1	1.1 ± 0.4	0.93
u	$> 26.5(3\sigma)$					
g	25.9 ± 0.3					
K_s	$> 23.3(3\sigma)$					

3.2 NOT/Alfosc imaging

We use *mag_{auto}* in SExtractor (Bertin & Arnouts 1996) to measure the total fluxes of SDSS stars in the u- and g-band images of the field of Q 0918+1636, which we use to derive the zeropoints. In order to do photometry of the DLA galaxy counterpart we first did PSF subtraction using the same procedure as in similar previous studies (e.g., Møller & Warren 1993; Fynbo et al. 1999, 2000). Magnitudes were measured in circular apertures. Again, Galactic extinction corrections are taken from the Schlafly & Finkbeiner (2011) maps. In the g-band we measure an AB magnitude of 25.9 ± 0.3 and in the u-band we do not detect the DLA galaxy down to a 3σ detection limit of 26.5 (in a 2 arcsec diameter aperture).

3.3 NOT/NOTCam imaging

For the NOTCam/ K_s -band we determined the zeropoint with stars from the 2MASS catalog (Skrutskie et al. 2006). On the combined image in the K_s -band we again subtracted the PSF of the QSO using a PSF determined from stars in the field. The residual image does not contain significant emission at the position of the $z = 2.583$ DLA galaxy. There is residual flux at the expected position at the 2σ significance level, but we conservatively report a 3σ detection limit of 23.3 (on the AB system) measured in a 2 arcsec diameter aperture.

3.4 SED fitting

We fit stellar population synthesis models to the six broad-band photometric points from the *HST* and NOT imaging listed in Table 2, to derive the stellar mass, age and star formation rate with the same procedure as in Krogager et al. (2013). In summary the fitting code uses the stellar population templates from Bruzual & Charlot (2003) convolved with a large Monte Carlo library of star formation histories (exponential plus random bursts) assuming a Chabrier (2003) IMF. Dust is added following the two-component model of Charlot & Fall (2000), with the parameters being the total optical depth, τ_v , and the fraction of dust³ contributed by the ISM, μ . The metallicity is restricted to solar as inferred from the absorption analysis, but we find consistent results when using the full range of the models between 20% and 2.5 times solar. We then adopt a Bayesian approach by comparing the observed magnitudes to the ones predicted by all the models in the library, and we construct

³ For details on the prior distribution of the SFH and dust parameters see Salim et al. (2005)

Table 3. Results from the SED fitting

Parameter	Value
Age [Myr]	233^{+268}_{-125}
E_{B-V} [mag]	$0.38^{+0.16}_{-0.12}$
A_V [mag]	$1.54^{+0.72}_{-0.56}$
M_* [$10^9 M_\odot$]	$12.6^{+6.1}_{-2.9}$
SFR [$M_\odot \text{yr}^{-1}$] ¹	27^{+20}_{-9}

¹ Averaged over 1 Gyr, but averaged over a shorter timescale of 10 Myr we get a similar value within the errors.

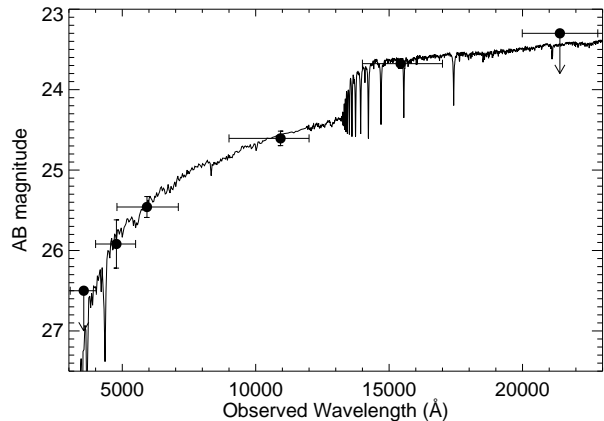


Figure 3. The broad-band SED of the $z = 2.583$ DLA galaxy, comprising of the Alfosc u- and g-bands, HST/WFC3 F606W-, F105W- and F160W-bands and the NOTCam K_s -band, is shown as black points. The best-fit model is shown with a full-drawn line.

the probability density functions of stellar mass, mean luminosity-weighted stellar age, and star formation rate. Fortunately, none of the filters contains any of the strong emission line and hence we do not include emission lines in the fits. The results of the SED-fits are provided in Table 3.

3.5 VLT/X-Shooter spectroscopy

The galaxy which is responsible for the $z = 2.583$ DLA is located at a projected distance of $1''.98$ from the QSO, which corresponds to 10 pixels on the spatial axis of the 2D spectrum. Given the good seeing of $0''.8$ the two objects are well separated. Thus, we do not need to subtract the continuum of the QSO. At the spatial position where the DLA galaxy is located, there is very little continuum

flux, but the [OIII] $\lambda 5007$ emission line of the $z = 2.583$ DLA galaxy is clearly visible. The [OIII] $\lambda 5007$ line is typically the line detected at highest S/N ratio for galaxies at similar redshifts (e.g., Fynbo et al. 2011). We then extract a 1D spectrum of the $z = 2.583$ DLA galaxy similarly as for the QSO spectrum, but this time using a gaussian SPSF with a FWHM of $0''.8$, as there is not enough continuum signal to determine the SPSF. The [OIII] $\lambda 5007$ emission line is clearly located in wavelength regions without sky-line residuals. For this line the flux is determined by summing up the flux in the 1D spectrum. In Fig 4 we show the [OIII] $\lambda 5007$ line in 1 and 2 dimensions. The redshift determined from the [OIII] $\lambda 5007$ line is $z = 2.58277 \pm 0.00010$, which is $36 \pm 20 \text{ km s}^{-1}$ (where the uncertainty also includes the uncertainty on the absorption redshift) blueshifted compared to the centre of the low-ionisation absorption lines (Fynbo et al. 2011).

To search for emission at lower impact parameter we subtract the QSO continuum following the procedure described in Fynbo et al. (2010). In Fig. 5 we show a wider region around the [OIII] $\lambda 5007$ line from the $z = 2.583$ DLA galaxy after subtraction of the SPSF of the QSO. There is no evidence for emission at smaller impact parameters.

The $H\alpha$, $H\beta$, [OIII] $\lambda 4960$, and [OII] $\lambda 3727$ lines are visible but detected at lower S/N ratio. We derive fluxes for these lines by fixing the redshift and width from the [OIII] $\lambda 5007$ line. The resulting line fluxes are provided in Table 5. In particular $H\alpha$ is very uncertain as it is located far in the red end of the K-band where the sky-background is very high. We use the emission-line ratio R_{23} (originally defined by Pagel et al. (1979)) to derive the oxygen abundance for the system. The index is defined as the ratio of [OII] $\lambda 3727$ and [OIII] $\lambda\lambda 4959,5007$ to $H\beta$. The R_{23} metallicity indicator is double-valued. Moreover, the calibration of the line ratio depends on the ionization parameter, which also depends on metallicity. We therefore solve the problem iteratively by use of the line ratio O_{32} as an indicator of the ionization parameter. By using the calibration of Kobulnicky & Kewley (2004) to infer the metallicity, we obtain the following two values: the upper branch solution is $12 + \log(O/H) = 8.8 \pm 0.2$, and the lower branch solution is $12 + \log(O/H) = 8.2 \pm 0.2$. We consider the upper branch solution most likely in this case given the other properties of the system (absorption metallicity, luminosity, mass), but we cannot establish this on the basis of the emission lines alone.

For the $H\alpha$ emission line the observed line flux corresponds to a luminosity of $L_{H\alpha} = 1.5 \pm 0.5 \times 10^{42} \text{ erg s}^{-1}$. Converting the luminosity into SFR using Kennicutt (1998) gives $\text{SFR}_{H\alpha} = 13 \pm 5 M_{\odot} \text{ yr}^{-1}$. Converting to the assumed Chabrier IMF (Treyer et al. 2007) we find $\text{SFR}_{H\alpha} = 8 \pm 3 M_{\odot} \text{ yr}^{-1}$. Correcting for the extinction inferred from the SED fitting this corresponds to $22 \pm 7 M_{\odot} \text{ yr}^{-1}$ for the Chabrier IMF, consistent with the SFR derived from the SED fitting in Table 3.

Due to the increased S/N ratio of the spectrum of Q0918+1636 we are also able to detect much weaker absorption lines than in Fynbo et al. (2011). An example is TiII $\lambda 1910$ for which we measure an observed equivalent width of $0.102 \pm 0.014 \text{ \AA}$ corresponding to a metallicity of -0.98 ± 0.05 implying that Titanium is depleted by close to 1 dex. This is consistent with observations of Titanium in the local group where Titanium is found to be highly depleted onto dust grains (e.g., Welty & Crowther 2010). It is also consistent with the large depletion of Fe, Mn and Cr (Fynbo et al. 2011).

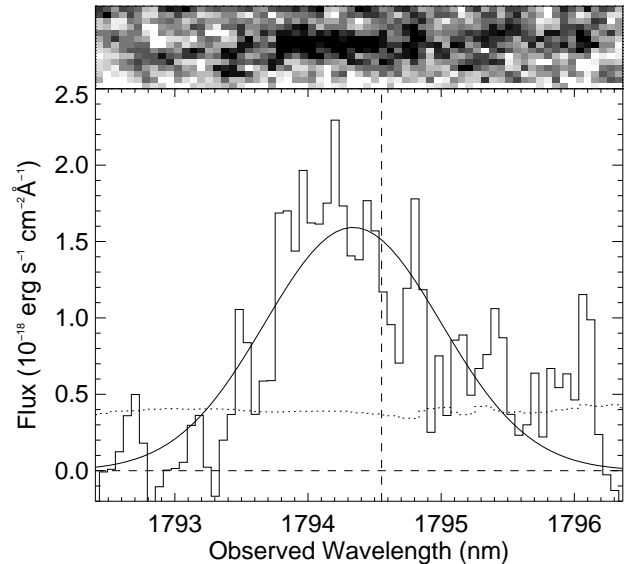


Figure 4. The [OIII] $\lambda 5007$ emission line of the $z = 2.583$ DLA galaxy. The top panel shows the 2D spectrum and the bottom panel shows the 1D spectrum. The vertical dashed line indicates the predicted position of the line based on the absorption line redshift of the DLA. The observed line has a centroid that is blue shifted by 36 km s^{-1} relative to the absorption redshift. The FWHM of the line based on a Gaussian fit is $256 \pm 23 \text{ km s}^{-1}$ (uncorrected for the spectroscopic resolution of 45 km s^{-1}).



Figure 5. A wider region around the [OIII] $\lambda 5007$ line of the $z = 2.583$ DLA galaxy after subtraction of the QSO SPSF (the boundaries of where the QSO continuum has been subtracted can be seen at each end of the figure). As seen here, there is no evidence for [OIII] $\lambda 5007$ emission at small impact parameter. A [OIII] $\lambda 5007$ line 3 times fainter than the detected line would have been detected even if superposed on the QSO trace.

4 THE $z = 2.412$ DLA GALAXY

4.1 Absorption line analysis

The original reason for targeting this QSO was the presence of a metal-strong DLA at $z = 2.412$. To characterize the absorption line properties of the $z = 2.412$ DLA we performed Voigt-profile fitting of the HI and metal absorption lines. For the DLA we derive an HI column density of $\log N/\text{cm}^{-2} = 21.26 \pm 0.06$ (Fig. 6).

Voigt-profiles were fitted to several metal lines using the VPFIT software⁴, assuming turbulence-dominated internal motion in the system. The redshift measured from the low-ionization (SiII, FeII, ZnII, CrII, MnII) absorption lines is $z = 2.4121 \pm 0.0002$. Redshifts and velocity dispersions were tied for each of the individual components of the low-ionisation lines. High-ionisation lines were fitted independently. The low-ionization absorption was found to be best fitted by six distinct components. A plot of the fit results is shown in Fig. 7, and inferred column densities are shown in Table 4. Integrated metallicities [M/H] based on low-ionization absorption are -0.6 ± 0.2 , -0.6 ± 0.2 , -1.2 ± 0.2 , -1.2 ± 0.2 and -1.3 ± 0.2 for ZnII, SiII, CrII, FeII and MnII, respectively.

⁴ <http://www.ast.cam.ac.uk/rfc/vpfit.html>

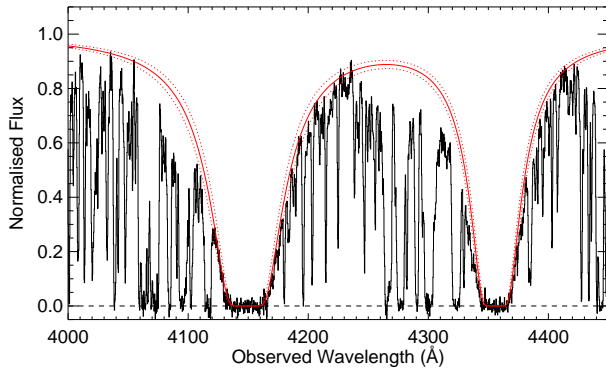


Figure 6. Voigt profile fits to the two DLA lines. For the $z = 2.583$ DLA at $\lambda = 4355 \text{ \AA}$ the fit is from Fynbo et al. (2011). The derived column density for the $z = 2.412$ DLA is $\log N/\text{cm}^{-2} = 21.26 \pm 0.06$.

In Fig. 7 we also show the intermediate and high-ionisation lines from AlIII and CIV. These lines are fitted independently and in this case only 5 sub-components suffice. It is striking that the $v < 0 \text{ km s}^{-1}$ absorption is strongest for AlIII and CIV whereas the strongest low-ionisation absorption is at $v > 0 \text{ km s}^{-1}$.

The resolution of X-Shooter is, as discussed in several earlier works, not ideal for robust Voigt-profile fitting (e.g., Fynbo et al. 2010; Noterdaeme et al. 2012a; Krühler et al. 2013), but for our purposes of establishing that the system is metal-rich and for inferring the velocity width of the absorption, the data are sufficient.

We also determine the velocity width of the low-ionisation absorption following the prescription of Ledoux et al. (2006). Here we find $\Delta v = 349 \text{ km s}^{-1}$ and 352 km s^{-1} for FeII, $\lambda 2260$ and SiII, $\lambda 1808$, respectively.

In conclusion, the metallicity of the system is well above our target selection criterion of $0.1 Z_{\odot}$ and there is evidence for substantial depletion of refractory elements on dust grains.

Further details on the analysis of this system can be found in Thorsen (2011).

4.2 The galaxy counterpart

In Fynbo et al. (2011) no emission was found from the galaxy counterpart of this absorber. From the spectrum taken with the slit at the position angle of 162° East of North we find that the galaxy seen at the bottom of Fig. 1 is at a lower redshift of $z = 0.987$ based on the detection of the [OII] $\lambda 3727$ doublet and the [OIII] $\lambda 5007$ line. In Fig. 2 there is no obvious other source at smaller impact parameters except the counterpart of the $z = 2.583$ DLA. One possibility is that the source is a faint galaxy at a small impact parameter. In the lower left sub-panel of the upper panel in Fig. 2 there is a hint of a source at a position angle of about 130° East of North (marked with an arrow). Opposite to this is a ring-like residual consistent with what one would expect if the centroid of the PSF has been shifted slightly to the lower left by the presence of the foreground galaxy. We have attempted to include such an additional source in the GALFIT modelling, but without success. We have done one test to gauge the reality of this potential source. Using GALFIT with rotated PSFs (45° , 90° , 135° , etc.), we find that the dimples surrounding the PSF core are either well subtracted or poorly subtracted (or, in general, partially subtracted) depending on the angle of rotation. Obviously, the main effect is that the diffraction spikes change such that with a rotation one sees the original

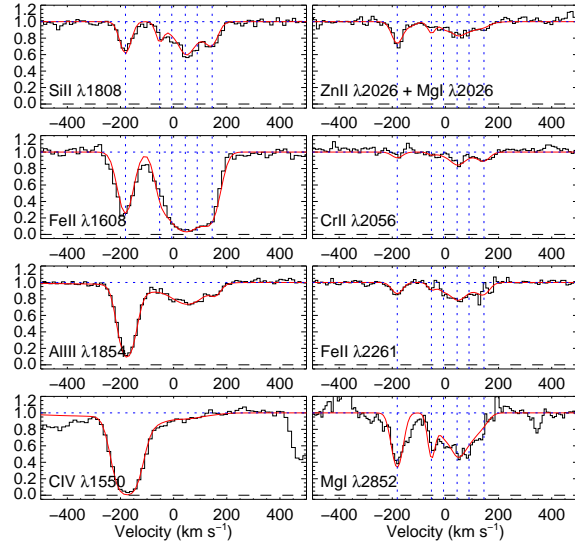


Figure 7. Voigt-profile fits to metal lines from the $z = 2.412$ DLA. The zero-point for the velocity scale is defined from the centroid of the [OIII] $\lambda 5007$ emission line. Data are shown in black and the model-fits in red. In the left column we list a weak and a strong low-ionisation line (SiII and FeII) and a medium- and high-ionisation line (AlIII and CIV) to illustrate the very different ionization states of the different sub-components. The vertical dotted lines mark the velocities for the sub-components in the fit to the low-ionisation lines. In the right column we show the low-ionisation lines from ZnII, CrII, FeII and MgI. The zero-point for the velocity scale is defined by the centroid (first moment) of the SiII 1808 line.

spikes as a positive residual and a negative residual oriented along the diffraction spikes of the rotated PSF. However, the residual to the south-east, labeled in the image, remains fixed with roughly the same shape and brightness. In the end we are convinced that the residual is due to a real source and not an artifact from poor PSF subtraction. We note that the residual could also be related to the host galaxy of the QSO. The tail extending below the QSO is a result of Charge Transfer Inefficiency.

In the case of a very small impact parameter we expect potential emission lines from the galaxy to be included in all the slits shown in Fig. 1. We therefore co-added all the 2-dimensional spectra obtained up to 2012 and performed a SPSF-subtraction as described in Fynbo et al. (2010). In the upper panel of Fig. 8 we show the region around the position in the spectrum where the [OIII] $\lambda 5007$ emission line is expected to fall. We tentatively, at about 3.5σ significance, detect an emission line at the expected position. The spectrum we obtained in March 2013 is substantially better due to better observing conditions and the use of the nodding observing template. In the lower panel of Fig. 8 we show the [OIII] $\lambda 5007$ emission line from the $z = 2.412$ DLA now at a higher S/N ratio. The line is very narrow with a FWHM of $67 \pm 12 \text{ km s}^{-1}$, which is only slightly larger than the resolution of 45 km s^{-1} . Corrected for the resolution the FWHM is 50 km s^{-1} . The redshift determined from the line is $z = 2.4128 \pm 0.0002$, which is redshifted $38 \pm 25 \text{ km s}^{-1}$ relative to the mean absorption redshift, but of course well within the full $\sim 350 \text{ km s}^{-1}$ velocity extent of the low-ionisation absorption.

We do not detect other lines, but [OIII] $\lambda 5007$ is the line expected to be detected at highest significance at these redshifts (e.g., Fynbo et al. 2010; Krühler et al. 2012, 2013) and the non-detection of the other lines is expected on S/N grounds.

Table 4. Ionic column densities in the 6 individual line components of the DLA system at $z_{\text{abs}} = 2.412$.

Ion	Transition lines used	$\log N \pm \sigma_{\log N}$	$b \pm \sigma_b$ (km s ⁻¹)
$z_{\text{abs}} = 2.41033$			
MgI	2026,2852	12.60±0.05	38±1
SiII	1808	15.40±0.05	38±1
MnII	2576,2594,2606	12.79±0.05	38±1
FeII	1608,1611,2249,2260	14.70±0.05	38±1
ZnII	2026, 2062	12.77±0.05	38±1
CrII	2056,2062,2066	12.80±0.10	38±1
$z_{\text{abs}} = 2.41179$			
MgI	2026,2852	12.34±0.07	20±3
SiII	1808	15.0±0.1	20±3
MnII	2576,2594,2606	11.9±0.2	20±3
FeII	1608,1611,2249,2260	14.29±0.08	20±3
ZnII	2026, 2062	12.3±0.1	20±3
CrII	2056,2062,2066	12.3±0.4	20±3
$z_{\text{abs}} = 2.41231$			
MgI	2026,2852	12.1±0.1	22±6
SiII	1808	15.3±0.7	22±6
MnII	2576,2594,2606	12.6±0.7	22±6
FeII	1608,1611,2249,2260	14.8±0.7	22±6
ZnII	2026, 2062	12.4±0.7	22±6
CrII	2056,2062,2066	12.9±0.8	22±6
$z_{\text{abs}} = 2.41289$			
MgI	2026,2852	12.4±0.5	37±11
SiII	1808	15.4±0.5	37±11
MnII	2576,2594,2606	12.6±0.6	37±11
FeII	1608,1611,2249,2260	14.9±0.5	37±11
ZnII	2026,2062	12.5±0.5	37±11
CrII	2056	13.2±0.3	37±11
$z_{\text{abs}} = 2.4134$			
MgI	2026,2852	12.4±0.6	45±28
SiII	1808	15.3±0.7	45±28
MnII	2576,2594,2606	12.6±0.7	45±28
FeII	1608,1611,2249,2260	14.8±0.7	45±28
ZnII	2026, 2062	12.4±0.7	45±28
CrII	2056,2062,2066	12.9±0.8	45±28
$z_{\text{abs}} = 2.41404$			
MgI	2026,2852	11.5±1.0	28±3
SiII	1808	15.2±0.2	28±3
MnII	2576,2594,2606	12.5±0.2	28±3
FeII	1608,1611,2249,2260	14.7±0.2	28±3
ZnII	2026, 2062	11.9±0.4	28±3
CrII	2056,2062,2066	13.0±0.1	28±3

The impact parameter is consistent with 0 and a conservative upper limit is 0.25 arcsec corresponding to 2.0 kpc.

5 DISCUSSION

In this paper we have presented new observations of the two DLAs towards Q0918+1636 and their galaxy counterparts. The galaxy counterpart of the $z = 2.583$ DLA was discovered previously (Fynbo et al. 2011), whereas the discovery of the counterpart of the $z = 2.412$ DLA is first reported here.

Table 5. Measured emission line fluxes

Transition	Wavelength ⁽¹⁾	Flux ⁽²⁾	FWHM ⁽³⁾
$z = 2.412$ DLA			
[O III]	5006.84	4.1±1.1	50±12
$z = 2.583$ DLA			
[O II]	3726.03, 3728.82	25±4	
[O III]	4958.92	11±3	
[O III]	5006.84	25±3	252 ± 23
H β	4861.325	13±3	
H α	6562.80	27±10	

(1) Transition rest frame wavelength in Å.

(2) Flux in units of 10^{-18} erg s⁻¹ cm⁻².

(3) Line width at FWHM in units of km s⁻¹ corrected for the instrumental resolution of 45 km s⁻¹.

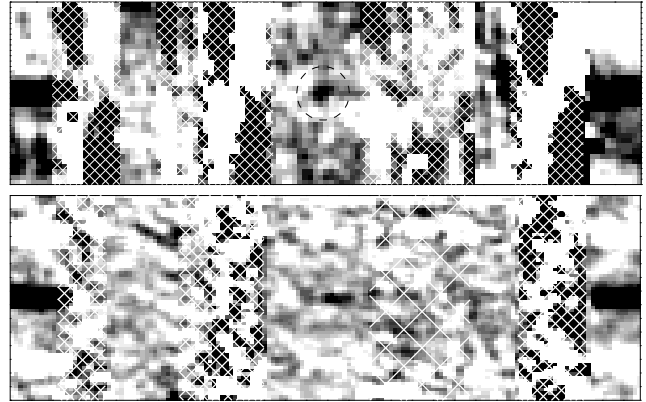


Figure 8. The region around the position in the spectrum where the [OIII] $\lambda 5007$ emission line from the $z = 2.412$ DLA galaxy is expected to be observed. The upper panel is based on a stack of all the data taken up to and including 2012 and the lower panel is based on the 3 hr observation from March 2013. The QSO continuum can be seen in the left and right extremes of the figures, but in between it has been subtracted. Regions with sky-lines from airglow have been marked with a double-hatched pattern. The [OIII] $\lambda 5007$ emission line from the $z = 2.412$ DLA galaxy is marked with a dashed circle in the upper panel.

5.1 The $z = 2.583$ DLA Galaxy

For the $z = 2.583$ DLA Galaxy we have the largest amount of information: detection of several strong emission lines and a clear detection of the galaxy in the *HST* images. We can use our information about the size of the galaxy and the kinematics, as probed by the [OIII] $\lambda 5007$ emission line of the $z = 2.583$ DLA galaxy to get an estimate of the dynamical mass of the system. As in Krogager et al. (2013) we follow the method described in Rhoads et al. (2013) to estimate the dynamical mass given the measured size and velocity dispersion:

$$M_{\text{dyn}} \approx \frac{4 \sigma^2 r_{\text{eff}}}{G \sin^2(i)},$$

where i denotes the inclination of the system with $i = 90^\circ$ being edge on and G is the gravitational constant. In order to estimate the velocity dispersion of the system we use the FWHM of the emission lines as a probe of the integrated gas-kinematics of the system. We then use the width of the [OIII] $\lambda 5007$ line to estimate the ve-

locity dispersion to be $\sigma = 107 \pm 10 \text{ km s}^{-1}$, and we adopt the size from the GALFIT analysis: $r_{\text{eff}} = 1.4 \text{ kpc}$ (see Table 2).

From the GALFIT analysis we infer a (projected) axis ratio of the galaxy of $b/a = 0.43$. The system may be described as disc-like, given the elongated shape, and the fact that we see a value of Sérsic n close to 1. We thus adopt a value of $\sin(i) = 0.5$ and use the fitted half-light semi-major axis for our estimate of the dynamical mass of the system: $M_{\text{dyn}} \approx 6.0 \pm 1.3 \times 10^{10} M_{\odot}$. This estimate should only be considered a rough approximation given the assumptions.

From our SED fit to the broad band imaging data, we obtain a stellar mass of $M_{\star} \gtrsim 10^{10} M_{\odot}$. We can use this measurement to test the mass-metallicity relation for DLA systems (Ledoux et al. 2006; Møller et al. 2013). Using the relation in Møller et al. (2013, their eq. 6) using as input solar metallicity (i.e., assuming that $C_{[M/H]} = 0$) we predict a stellar mass of $M_{\star} = 3 \times 10^{10} M_{\odot}$. Given the substantial (~ 0.38 dex) scatter in their relation, the agreement between the prediction and our best fit stellar mass from the SED fit is good.

5.2 The nature of DLA galaxies

The two DLA systems studied here are, as other systems in our survey (Fynbo et al. 2010, 2011; Krogager et al. 2012), drawn from the extreme high-metallicity end of the distribution and hence should not be considered typical examples of DLA galaxies. In Table 6 we compare the two systems and include also DLA galaxies from the literature for comparison (Weatherley et al. 2005; Fynbo et al. 2010, 2011; Bouché et al. 2012; Noterdaeme et al. 2012a; Krogager et al. 2013). For consistency we re-calculate the velocity shifts for N-14-1C and N-14-2C using the centroids of the low-ionisation lines corresponding to $z_{\text{abs}} = 1.9205$. The galaxy counterpart of the $z = 2.412$ DLA is the system with the highest velocity extent of the low-ionisation absorption. However, the FWHM of its [OIII] emission is the lowest in the sample. This indicates that additional influences than mass must be important in determining the velocity width of the low-ionisation absorption. One such possible influence is of course outflows. Another important reason for this may be the low impact parameter, which implies that a larger fraction of the gravitational potential is probed by the line-of-sight. We also observe here, as in Krogager et al. (2012), that the systems with the highest HI column densities have the smallest impact parameters. It would be interesting to carry out detailed comparisons of the quantities in Table 6 with simulations, e.g., similar to the works of Pontzen et al. (2008) and Rakic et al. (2013).

For the galaxy counterpart of the $z = 2.583$ we can establish further properties: It is a compact ($r_{\text{eff}} = 1 \text{ kpc}$), strongly star-forming galaxy with a centroid 16.2 kpc away from the line-of-sight to the background QSO. The galaxy photometry is well fitted by galaxy templates with ages up to several 100 Myr. The ratio between the HI gas scale length of this DLA galaxy, as measured by its impact parameter, and the light scale length, as measured by its half-light radii, is of order 10 as seen in previous cases of DLA galaxy counterparts (Møller et al. 2002; Krogager et al. 2013). This is very different from the situation in local galaxies, where the gas only extends up to a few times the extension of the light (Bosma 1981). Our data are deep, but the $(1+z)^4$ dimming of surface brightness with redshift is a very strong effect. Hence, an important question is whether the measured compact morphology is only due to central high surface brightness regions embedded in lower surface brightness regions with extension more similar to the HI gas, but below the surface brightness detection limit of our data. Such HI

central high surface brightness regions are also seen in local spiral galaxies (e.g., Carollo et al. 1997). The issue of morphology of star-forming galaxies at these redshifts as inferred from WFC3/IR data has been studied intensively by Law et al. (2012a,b) who find that these systems are not rotationally supported disk galaxies. Rather, they appear to be predominantly unstable, dispersion-dominated, systems fueled by rapid gas accretion which presumably later form extended rotationally supported disks. They also argue that all these galaxies drive strong outflows with more massive galaxies driving less highly ionized outflows. Compared to their sample the $z = 2.583$ DLA galaxy is in the upper third of the mass distribution. For the $z = 2.583$ galaxy the distances and ages are also consistent with a wind scenario: for an age of 233 Myr a mean speed of $\sim 70 \text{ km s}^{-1}$ is required to reach 16 kpc. Such wind speeds are well below what is seen in nearby (more modest) winds (e.g., Melioli et al. 2013).

Bouché et al. (2013) argue for a similar system of a galaxy counterpart to a DLA at an even larger impact parameter (DLA2243-60 in Table 6) that the gas causing the DLA absorption is in a cold inflow. In their case the DLA metallicity is -0.72 , which is too high to be pristine gas. Hence, also in this case, an outflow must have been important for determining the properties of the system.

Rafelski et al. (2011) use statistical arguments to show that most DLAs must probe atomic gas with very low star-formation efficiencies. This would be consistent with a picture where metals in this gas originates from a wind rather than having been formed in situ.

The large impact parameter of the $z = 2.583$ galaxy could also be related to other processes like tidal stripping similar to what is seen in the Magellanic stream (Misawa et al. 2009). As DLAs are HI cross-section selected such systems will have a higher probability of being selected (see also Rauch et al. 2011, 2013). However, we note that the correlation between metallicity and impact parameter found by Krogager et al. (2012) would not obviously result from such a scenario and we do not see evidence for a nearby galaxy that could have caused tidal stripping.

We note that none of the two galaxies have Ly α in emission. This may help explain the many non-detections resulting from searches for DLA galaxies in the previous few decades (Lowenthal et al. 1995; Møller et al. 2004; Fynbo et al. 2010, and references therein).

A coherent picture of DLAs and their relation to emission selected galaxies could be the following: DLAs originate from the outskirts of galaxies with properties (i.e., sizes, luminosities, stellar masses, metallicities) within the range of star-forming Lyman-break galaxies at similar redshift, but due to their cross-section selection they are more likely to be drawn from the fainter end of the luminosity function than emission selected galaxies (Fynbo et al. 1999; Møller et al. 2002; Fynbo et al. 2008; Rauch et al. 2008; Rauch & Haehnelt 2011). There is evidence that DLA galaxies fulfill a metallicity-luminosity relation (Møller et al. 2004; Ledoux et al. 2006; Fynbo et al. 2008; Møller et al. 2013) and therefore high-metallicity DLAs are expected to have galaxy counterparts more similar to typical emission-selected galaxies (i.e., Lyman-break galaxies seen in ground-based surveys) than DLAs in general which probably have extreme galaxy counterparts (Fynbo et al. 1999; Haehnelt et al. 2000; Rauch et al. 2008). The galaxy counterparts of the two DLAs towards Q0918+1636 are consistent with this picture.

Table 6. Comparison of the two DLA galaxies studied here with DLA galaxies at similar redshifts from the literature. In the table we refer to the $z = 2.412$ and $z = 2.583$ DLA galaxies as DLA0918+1636-1 and DLA0918+1636-2, respectively.

DLA galaxy	z_{abs}	$\log N/\text{cm}^{-2}$	[M/H]	b^1 (kpc)	FWHM([OIII]) (km s^{-1})	Δv_{90} (km s^{-1})	$\Delta v(\text{DLA}-[\text{OIII}])$ (km s^{-1})	ref
DLA0918+1636-1	2.412	21.26	-0.6	< 2	50	350	-38 ± 25	(1)
DLA0918+1636-2	2.583	20.96	0.0	16.2	252	295	-36 ± 20	(1)
DLA1135-0010	2.207	22.10	-1.1	0.9	120	186	9 ± 10	(2)
DLA2222-0946	2.353	20.65	-0.5	6.2	115	185	25 ± 20	(3)
N-14-1C	1.920	20.67	-0.4	8.3	220	136	-150 ± 20	(4)
N-14-2C	1.920	20.67	-0.4	10.6	180	136	80 ± 9	(4)
DLA2243-60	3.330	20.65	-0.7	22.9	320	173	200 ± 20	(5)

(1) This work, Fynbo et al. (2011); (2) Noterdaeme et al. (2012a); (3) Fynbo et al. (2010); Krogager et al. (2013); (4) Weatherley et al. (2005); Ledoux et al. (2006); (5) Bouché et al. (2012); Ledoux et al. (2006); Bouché et al. (2013), Noterdaeme, private communication.

¹ Recalculated from the values in the original references to be consistent with the assumed cosmology.

5.3 Outlook

Thanks to new sensitive near-IR spectrographs the study of galaxy counterparts of $z > 2$ DLAs has now opened (Weatherley et al. 2005; Fynbo et al. 2010, 2011; Bouché et al. 2012; Noterdaeme et al. 2012a; Krogager et al. 2013). The identification of intervening DLAs towards transient sources like Gamma-Ray Burst afterglows have also led to the detection of a galaxy counterpart and this approach hence also appears promising for the future (Schulze et al. 2012). At the moment observations like these are limited to the bright counterparts of the highest metallicity DLAs. With the advent of extremely large telescopes equipped with advanced adaptive optics in the next decade, however, such studies can be extended to the galaxy counterparts of more typical DLAs and hence a more complete unification of absorption and emission studies of high- z galaxies is within reach.

ACKNOWLEDGMENTS

We thank the anonymous referee for a very help report and Steve Schulze for comments on an earlier version of the manuscript. The Dark Cosmology Centre is funded by the DNRF. JPUF acknowledges support from the ERC-StG grant EGGS-278202. LC acknowledges the support of the EU under a Marie Curie Intra-European Fellowship, contract GA-2010-247117. AG acknowledges support from the EU FP7/2007-2013 under grant agreement n. 267251 AstroFit. The research of JRM is supported through a Royal Society University Research Fellowship. TK acknowledges support by the European Commission under the Marie Curie Intra-European Fellowship Programme in FP7.

REFERENCES

- Bertin, E. & Arnouts, S., 1996, *A&AS*, 117, 393
 Bosma, A., 1981, *AJ*, 86, 1825
 Bouché, N., Dekel, A., Genzel, R., et al., 2010, *ApJ*, 718, 1001
 Bouché, N., Murphy, M. T., Kacprzak, G. G., Péroux, C., Contini, T., Martin, C., & Dessauges-Zavadsky, M., 2013, *Science*, in press (arXiv:1306.0134)
 Bouché, N., Murphy, M. T., Péroux, C., et al., 2012, *MNRAS*, 419, 2
 Bruzual, G. & Charlot, S., 2003, *MNRAS*, 344, 1000
 Carollo, C. M., Stiavelli, M., de Zeeuw, P. T., & Mack, J., 1997, *AJ*, 114, 2366
 Chabrier, G., 2003, *Publications of the Astronomical Society of the Pacific*, 115, 763
 Charlot, S. & Fall, S. M., 2000, *ApJ*, 539, 718
 Crighton, N., Hennawi, J. F., & Prochaska, J. X., 2013, submitted to *ApJL*
 Dekel, A., Birnboim, Y., Engel, G., et al., 2009, *Nature*, 457, 451
 Dekel, A. & Krumholz, M. R., 2013, *MNRAS*, 432, 455
 Fumagalli, M., Prochaska, J. X., Kasen, D., Dekel, A., Ceverino, D., & Primack, J. R., 2011, *MNRAS*, 418, 1796
 Fynbo, J. P. U., Krogager, J.-K., Venemans, B., Noterdaeme, P., Vestergaard, M., Møller, P., Ledoux, C., & Geier, S., 2013, *ApJS*, 204, 6
 Fynbo, J. P. U., Laursen, P., Ledoux, C., et al., 2010, *MNRAS*, 408, 2128
 Fynbo, J. P. U., Ledoux, C., Noterdaeme, P., et al., 2011, *MNRAS*, 413, 2481
 Fynbo, J. P. U., Prochaska, J. X., Sommer-Larsen, J., Dessauges-Zavadsky, M., & Møller, P., 2008, *ApJ*, 683, 321
 Fynbo, J. U., Burud, I., & Møller, P., 2000, *A&A*, 358, 88
 Fynbo, J. U., Møller, P., & Warren, S. J., 1999, *MNRAS*, 305, 849
 Giavalisco, M., 2002, *ARA&A*, 40, 579
 Goldoni, P., 2011, *Astronomische Nachrichten*, 332, 227
 Haehnelt, M. G., Steinmetz, M., & Rauch, M., 2000, *ApJ*, 534, 594
 Horne, K., 1986, *PASP*, 98, 609
 Kennicutt, Jr., R. C., 1998, *ARA&A*, 36, 189
 Kobulnicky, H. A. & Kewley, L. J., 2004, *ApJ*, 617, 240
 Komatsu, E., Smith, K. M., Dunkley, J., et al., 2011, *ApJS*, 192, 18
 Krogager, J.-K., Fynbo, J. P. U., Ledoux, C., et al., 2013, *MNRAS*, 433, 3091
 Krogager, J.-K., Fynbo, J. P. U., Møller, P., Ledoux, C., Noterdaeme, P., Christensen, L., Milvang-Jensen, B., & Sparre, M., 2012, *MNRAS*, 424, L1
 Krühler, T., Ledoux, C., Fynbo, J. P. U., et al., 2013, *A&A*, 557, A18
 Krühler, T., Malesani, D., Milvang-Jensen, B., et al., 2012, *ApJ*, 758, 46
 Law, D. R., Steidel, C. C., Shapley, A. E., Nagy, S. R., Reddy, N. A., & Erb, D. K., 2012a, *ApJ*, 759, 29
 —, 2012b, *ApJ*, 745, 85
 Ledoux, C., Petitjean, P., Fynbo, J. P. U., Møller, P., & Srianand,

- R., 2006, *A&A*, 457, 71
- Lowenthal, J. D., Hogan, C. J., Green, R. F., Woodgate, B., Caulet, A., Brown, L., & Bechtold, J., 1995, *ApJ*, 451, 484
- Melioli, C., de Gouveia Dal Pino, E. M., & Geraissate, F. G., 2013, *MNRAS*, 430, 3235
- Misawa, T., Charlton, J. C., Kobulnicky, H. A., Wakker, B. P., & Bland-Hawthorn, J., 2009, *ApJ*, 695, 1382
- Møller, P. & Warren, S. J., 1993, *A&A*, 270, 43
- Modigliani, A., Goldoni, P., Royer, F., et al., 2010, in *Society of Photo-Optical Instrumentation Engineers (SPIE) Conference Series*, Vol. 7737, *Society of Photo-Optical Instrumentation Engineers (SPIE) Conference Series*
- Møller, P., Fynbo, J. P. U., & Fall, S. M., 2004, *A&A*, 422, L33
- Møller, P., Fynbo, J. P. U., Ledoux, C., & Nilsson, K. K., 2013, *MNRAS*, 430, 2680
- Møller, P., Warren, S. J., Fall, S. M., Fynbo, J. U., & Jakobsen, P., 2002, *ApJ*, 574, 51
- Noterdaeme, P., Laursen, P., Petitjean, P., et al., 2012a, *A&A*, 540, A63
- Noterdaeme, P., Petitjean, P., Carithers, W. C., et al., 2012b, *A&A*, 547, L1
- Pagel, B. E. J., Edmunds, M. G., Blackwell, D. E., Chun, M. S., & Smith, G., 1979, *MNRAS*, 189, 95
- Peng, C., 2010, in *Bulletin of the American Astronomical Society*, Vol. 42, *American Astronomical Society Meeting Abstracts #215*, p. 229.09
- Peng, C. Y., Ho, L. C., Impey, C. D., & Rix, H.-W., 2002, *AJ*, 124, 266
- Pontzen, A., Governato, F., Pettini, M., et al., 2008, *MNRAS*, 390, 1349
- Rafelski, M., Wolfe, A. M., & Chen, H.-W., 2011, *ApJ*, 736, 48
- Rakic, O., Schaye, J., Steidel, C. C., Booth, C. M., Dalla Vecchia, C., & Rudie, G. C., 2013, *MNRAS*, 433, 3103
- Rauch, M., Becker, G. D., Haehnelt, M. G., & Gauthier, J.-R., 2013, *ArXiv e-prints*
- Rauch, M., Becker, G. D., Haehnelt, M. G., Gauthier, J.-R., Ravindranath, S., & Sargent, W. L. W., 2011, *MNRAS*, 418, 1115
- Rauch, M., Haehnelt, M., Bunker, A., et al., 2008, *ApJ*, 681, 856
- Rauch, M. & Haehnelt, M. G., 2011, *MNRAS*, 412, L55
- Rhoads, J. E., Malhotra, S., Finkelstein, S. L., Fynbo, J. P. U., McLinden, E. M., Richardson, M. L. A., & Tilvi, V. S., 2013, *ArXiv e-prints*, 1301.3140
- Salim, S., Charlot, S., Rich, R. M., et al., 2005, *ApJL*, 619, L39
- Schlafly, E. F. & Finkbeiner, D. P., 2011, *ApJ*, 737, 103
- Schulze, S., Fynbo, J. P. U., Milvang-Jensen, B., et al., 2012, *A&A*, 546, A20
- Shapley, A. E., 2011, *ARA&A*, 49, 525
- Skrutskie, M. F., Cutri, R. M., Stiening, R., et al., 2006, *AJ*, 131, 1163
- Thorsen, T. J., 2011, Master's thesis, Niels Bohr Institute, Copenhagen University, Juliane Maries Vej 30, DK-2100 Copenhagen O, Denmark
- Treyer, M., Schiminovich, D., Johnson, B., et al., 2007, *ApJS*, 173, 256
- Weatherley, S. J., Warren, S. J., Møller, P., Fall, S. M., Fynbo, J. U., & Croom, S. M., 2005, *MNRAS*, 358, 985
- Welty, D. E. & Crowther, P. A., 2010, *MNRAS*, 404, 1321
- Weymann, R. J., Carswell, R. F., & Smith, M. G., 1981, *ARA&A*, 19, 41
- Wolfe, A. M., Gawiser, E., & Prochaska, J. X., 2005, *ARA&A*, 43, 861